1991

# Streams with moving contact lines: complex dynamics due to contact-angle hysteresis

M. A. Rubio
*Haverford College*

B. J. Gluckman

A. Dougherty
*Haverford College*

Jerry P. Gollub
*Haverford College*

PHYSICAL REVIEW A VOLUME 43, NUMBER 2 15 JANUARY 1991

# Streams with moving contact lines: Complex dynamics due to contact-angle hysteresis

Miguel A. Rubio
*Department of Physics, Haverford College, Haverford, Pennsylvania 19041*
*and Departamento de Física Fundamental, Universidad Nacional de Educación a Distancia,*
*Apartado Correos 60141, Madrid 28080, Spain*

Bruce J. Gluckman
*Department of Physics, Haverford College, Haverford, Pennsylvania 19041*
*and Department of Physics, University of Pennsylvania, Philadelphia Pennsylvania 19104*

A. Dougherty
*Department of Physics, Haverford College, Haverford, Pennsylvania 19041*
*and Department of Physics, Lafayette College, Easton, Pennsylvania 18042*

J. P. Gollub
*Department of Physics, Haverford College, Haverford, Pennsylvania 19041*
*and Department of Physics, University of Pennsylvania, Philadelphia, Pennsylvania 19104*
(Received 3 August 1990)

We have investigated experimentally the spatiotemporal behavior of a narrow water stream flowing between two parallel inclined Plexiglass plates bounded laterally by air. Complex broadband dynamics occurs as a result of the velocity dependence of the contact angle at the water-air-Plexiglass contact line, which introduces critical values into the pressure required for contact line motion over the Plexiglass plates. This mechanism causes a stick-slip type of motion similar to that appearing in other systems such as flows in granular materials, models of earthquake dynamics, and charge-density-wave motion in solids. We find that above a certain flow rate $Q_s$, a stationary spatial modulation of the width of the stream appears. At higher flow rates, a hysteretic transition occurs in which the contact line begins to move, and the pattern slips down the plates with broadband dynamics. The statistical properties of the motion are presented.

## I. INTRODUCTION

Complex spatiotemporal behavior is of considerable interest due to its appearance in many fields of science. Even within condensed-matter physics, several distinct types of spatiotemporal dynamics have been investigated. For instance, in deterministic systems with well-defined cellular patterns, the transition to one-dimensional spatiotemporal intermittency[1–3] and the transition between ordered and disordered two-dimensional structures have been investigated.[4] Complex spatiotemporal dynamics also occurs in discrete deterministic models (cellular automata) in which there are no characteristic time or length scales, such as those giving rise to "self-organized critical states."[5] This work has stimulated research on systems that show avalanching behavior such as sandpiles,[6–8] earthquakes,[9] and droplets on inclined surfaces.[10] These situations may be contrasted with others in which random perturbations need to be included to explain complex dynamics. An example of the latter is the motion of charge-density waves (CDW) in solids,[11] for which the more successful approaches include the pinning of the phase of the wave by random impurities in the material.[12,13]

Some of these systems share the characteristic of showing pinning of the objects that form the system. For instance, in the sandpile experiments of Jaeger, Liu, and Nagel,[6] avalanches start when the slope of the sandpile is equal to a certain critical angle $\theta_m$. This critical value is significantly higher than the final metastable equilibrium angle $\theta_r$. The pile is at rest until $\theta_m$ is attained; then it starts moving and stays in motion for the whole range of inclinations between $\theta_m$ and $\theta_r$. Analogous characteristics appear in the earthquake model of elastically coupled blocks considered by Carlson and Langer,[9] where the frictional force decreases with increasing velocity. Behavior similar to this "stick-slip" dynamics is also present in some models for CDW motion,[13] where the central feature is a hysteretic depinning transition for the phase of the wave as a function of applied voltage. For all of these systems, irregular and intermittent motion occurs at various length scales.

Stick-slip behavior is also known to occur in some hydrodynamic systems with moving contact lines at a solid surface.[14,15] Therefore it is natural to suspect that complex spatiotemporal dynamics can occur as a consequence. In this paper, we report an experimental investigation of a hydrodynamic system in which the stick-slip behavior of contact lines gives rise to broadband dynamics. The system is a water stream flowing by the action of gravity through the narrow gap between two parallel inclined plates that confine the stream above and below.

 

The stream is open to air laterally. When a substantial range of contact angles exists over which the contact line does not move, as occurs with water on Plexiglass, an instability leading to a spatially periodic (but time-independent) modulation of the width of the stream appears above a certain flow rate $Q_s$ (Fig. 1). We are not aware of previous reports of this instability, which is different from the surface-tension-induced instability of a free stream. If the flow rate is increased, a second threshold is found beyond which the width of the stream becomes time dependent and portions on the contact line are intermittently in motion. In this regime, the wide and narrow regions (necks) of the stream travel at an irregular rate down the channel, sometimes merging with other regions. The transition to erratic time dependence is hysteretic.

The problem of a stream flowing over a single plate has also received some attention.[16] In that case, the stream width is not strongly modulated, but the direction meanders (on a sufficiently long plate) and does not follow a straight course. The depinning of the meanders has been considered by Bruinsma, and this process may be related to the one under consideration. However, the presence of two plates in the present investigation fixes the stream thickness, and this appears to modify the dynamics substantially.

A useful characteristic of this system is that its spatiotemporal behavior can be adequately described for some purposes by the lateral width $w(x,t)$, a one-dimensional function of the downstream coordinate. The study of spatiotemporal dynamics requires the measurement of long-time statistical properties such as power spectra and probability distribution functions. It is difficult to compute these quantities adequately in more than one spatial dimension, so the effectively one-dimensional nature of the phenomenon is advantageous.

The paper is organized as follows. In Sec. II we describe the experimental configuration, contact-angle measurements, and image processing methods. Section III contains a general survey of the observed phenomena, and Sec. IV presents a more detailed study of the regime of broadband dynamics (sometimes also called spatiotemporal chaos). Finally, in Sec. V we summarize the results, discuss their relationship to other experiments and model systems, and comment on some unresolved aspects of the problem.

## II. EXPERIMENTAL SETUP, CONTACT-ANGLE MEASUREMENTS, AND DATA PROCESSING

### A. Stream instabilities

The experimental system consists of two rigidly clamped plates $122 \times 30$ cm$^2$, separated by a Teflon gasket of thickness $b = 0.105$ cm. The plates are inclined at an angle $\alpha$ with respect to the horizontal. We have employed two different pairs of plates with different wetting properties. The first set is ordinary plate glass 0.4 cm thick. Water wets clean glass well, so that the contact angle is very small and nearly independent of the velocity of the contact line. The glass plates do not show the instabilities that are the subject of this paper. Complex dynamical behavior was obtained with Plexiglass plates 1 cm thick. The important characteristic that distinguishes the Plexiglass from the glass plates is the presence of strong velocity dependence of the contact angle, and particularly, a vertical step at zero velocity. In all cases the plates are prepared by soaking them in a soap solution (Decontam; Electronic Space Products International) for 1 h, thoroughly rinsing with distilled water, and drying by nitrogen-glass flow. These steps were necessary to obtain reasonably uniform and reproducible wetting behavior.

The Teflon spacer is made in several pieces (Fig. 2) to allow for free flow of air on both sides of the stream. Therefore, the exterior of the stream is always at atmospheric pressure. The gasket is shaped to form a circular cavity into which the fluid can be injected through a hole in the plate. The fluid is water containing a small amount of uranine fluorescent dye (100 ppm) for visualization purposes. The fluid enters the main experimental region after flowing through an entry channel 10 cm long and 0.2 cm wide; the width of the channel is chosen to match the width of the free stream approximately in the absence of any instability. After traversing the apparatus, the fluid freely escapes through an outlet. The escaping fluid is recirculated into a large reservoir that provides a constant pressure head for the system. The flow rate is regulated by a needle valve and measured with a calibrated flowmeter having an overall readout precision of 0.02 cm$^3$/s, which is approximately equal to the long-term stability of the flow rate.

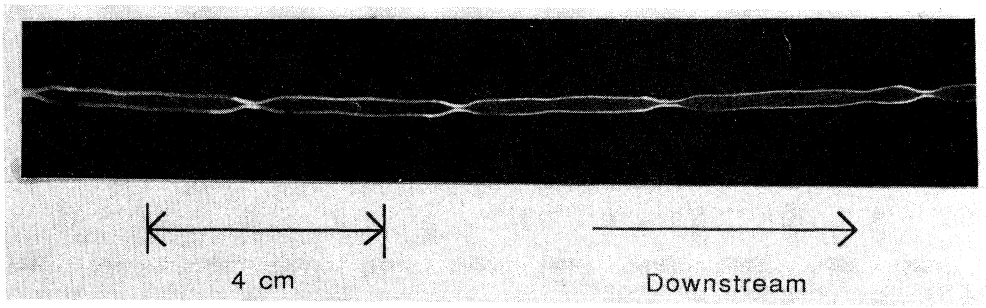


FIG. 1. Photograph of the stream in the stationary modulated regime. The angle of inclination is $\alpha = 19°$, and the flow rate is $Q = 0.28$ cm$^3$/s.

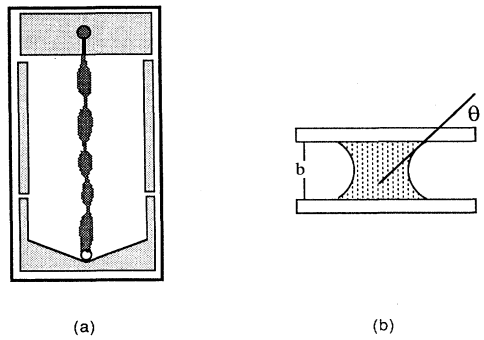


FIG. 2. Sketch of the experimental setup. (a) Top view of the cell showing details of the entrance region and the flow modulation. (b) Sketch of the stream cross section, showing the geometry and contact-angle definition.

We illuminate the stream with near ultraviolet light, thereby obtaining a fluorescent image of the stream, and record the dynamics with a video camera (MTI-CCD/71). The camera is located above the stream and away from the ends of the apparatus, in order to avoid possible edge and border effects. The magnification has been chosen as a compromise between obtaining sufficient spatial resolution transverse to the stream, and maintaining a sufficient length of the stream in the field of view. Typical values are 13 cm for the length of the observed region, and 0.02 cm for the resolution in the width measurements. The images are recorded and subsequently digitized by an Imaging Technologies Series 151 image processing system in a Sun 3/160 computer, with $512\times480$ pixels of spatial resolution, and 8 bits of intensity resolution. Typically the intensity variation across the water-air interface is high enough that a simple intensity threshold is sufficient to determine the interface position.

In the time-dependent regimes the stream width $w(x,t)$ is determined as a function of position downstream and time at 0.2-s intervals. This time is short enough to capture all the dynamical information. The digitized pictures themselves are not retained. The power spectra of the width at different positions $x_0$ are obtained by computing Fourier transforms of time series containing at least 8192 points.

We are also able to measure the trajectories of individual fronts, the junctions between wide and narrow stream segments, as defined by a width threshold. The positions of individual fronts can be measured to a precision better than 1% in most cases. This capability is useful for monitoring the repetitive stopping and starting of the fronts in the complex dynamical regime.

### B. Contact-angle measurements

The contact-angle measurements are carried out in a separate small rectangular cell built with the same materials as the plates used in the stream experiment. The horizontal dimensions of this cell are $10\times6$ cm$^2$. Contact angles are known to be dependent on the experimental geometry[17] (for example, the size of the gap), so the measurements are made in a geometry similar to that used for the stream flow experiments. The fluid is injected into the cell through a hole in one of the plates in order to minimize any direct influence of the injection on the air-water interface. The fluid fills the full width of this cell, and the injection rate is set by a syringe driven by high-precision stepper motor controller.

The cell is placed horizontally on the observation stage of an inverted microscope, and images are recorded with a video camera. When illuminated by transmission, the water-air interface appears as a dark band. In the absence of gravitational effects, the shape of the interface is an arc of a circle, so the thickness $\delta$ of this band is related to the contact angle by[17]

$$\delta=\frac{b}{2}\left[\frac{1}{\cos(\theta)}-\tan(\theta)\right].$$

The digital imaging system was used to obtain images of the interfaces, both at rest and when moving, and at different advancing and receding velocities. Figure 3 displays images of (a) advancing and (b) receding interfaces moving between plexiglass plates. The difference in apparent thickness of the interface (which reflects the contact-angle variation) may be clearly seen. After making background corrections from the digitized images, we obtain $\delta$ (which is needed to obtain $\theta$) as an average of distances across the dark band, defined by lines locally perpendicular to the boundaries. The local interfacial velocity is obtained by averaging perpendicular distances between two video frames.

The dependence of the contact angle on interfacial velocity is shown in Fig. 4 for the Plexiglass and glass plates. For glass, the contact angle is very small, but the method used gives an apparent value of approximately

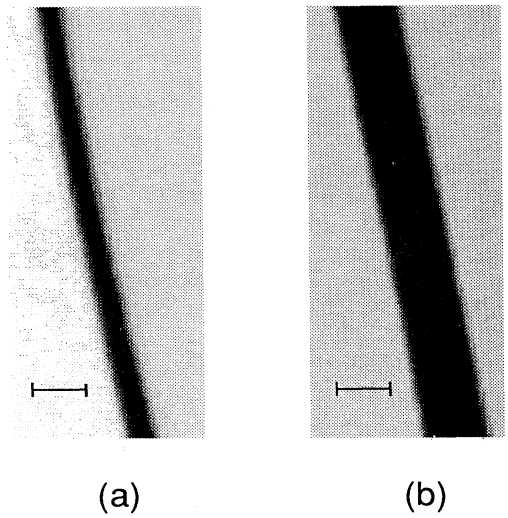


FIG. 3. Images of the advancing (a) and receding (b) interfaces between Plexiglass plates in the cell used to measure the contact angle. The scale bar is 0.2 mm. The interfacial velocity is 0.115 mm/s. Positive velocity is to the right, with fluid on the left side of the dark band, and air on the right side. From the apparent widths of these interfaces we compute the apparent contact angle.

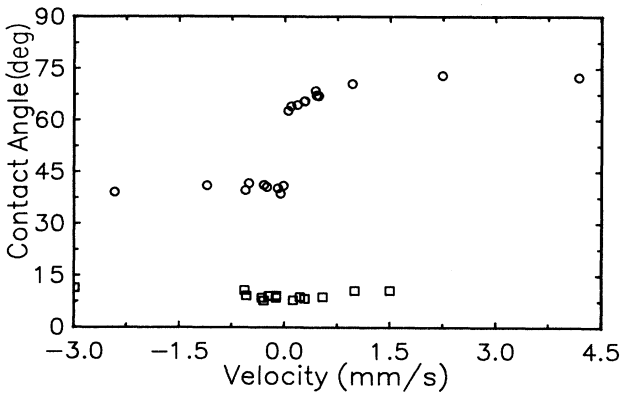


FIG. 4. Dependence of the contact angle on the interfacial velocity for Plexiglass plates (circles) and clean glass plates (squares). The contact angle is multivalued at $v=0$ for Plexiglass.

10°. The important observation is the relative velocity independence of the contact angle for glass. This behavior may be contrasted with the Plexiglass surfaces, for which there is a large difference between the contact angles for advancing (positive) and receding (negative) velocities. Equivalently, the contact angle at zero velocity is multivalued for Plexiglass.

## III. SURVEY OF OBSERVED PHENOMENA

We investigated the behavior of the system by varying two control parameters: the inclination angle $\alpha$, and the flow rate $Q$. At each value of $\alpha$, the flow rate was increased in steps of 0.05 $cm^3/s$. After each step the system was allowed to relax to a steady state. The longest transients were approximately 10 min; we generally waited at least 30 min. For each inclination, $Q$ was first increased and then decreased.

For each inclination four different regimes were found. For very small $Q$ a continuous stream does not exist; instead, drops are periodically formed at the cell entrance. In the second "constant-width regime," starting at a flow rate $Q_{CW}$, the stream is straight, fairly uniform in width, and time independent. The width may be locally perturbed by surface imperfections at positions that differ from run to run. No hysteresis was found for the threshold $Q_{CW}$.

Further increase in the flow rate to $Q_s$ leads to an instability in which the stream develops a spatial modulation of its width as shown in Fig. 1. The stream consists of alternating wide and narrow regions; the width of the narrow regions (necks) is close to the width of the stream in the constant-width regime. The wide regions are definitely longer than the narrow ones, and the structure is generally symmetric with respect to the center line of the stream. We refer to the downstream and upstream edges of a wide region as the leading and trailing fronts, respectively. Usually the spatial structure is not perfectly periodic, but the mean distance between necks appears to be independent of the position downstream, and an average wavelength $\lambda$ may therefore be defined. We find that $\lambda$ is roughly independent of the flow rate within the experimental error. (However, the domain in $Q$ of the stationary modulated structure is fairly small, so a weak dependence could easily be missed.) On the other hand, the variation of $\lambda$ with $\sin(\alpha)$ is roughly linear, ranging from 5.2 cm at $\alpha=9°$ to 2.2 cm at 24°. Any hysteresis in $Q_s$ is smaller than our step size, roughly 0.05 $cm^3/s$.

Complex time dependence occurs in a fourth regime, in which the wide regions begin to slide down the plates. We illustrate this behavior in Fig. 5, which consists of successive images separated by $\frac{1}{6}$ s at $\alpha=14°$ and $Q=0.86$ $cm^3/s$. The fronts or transition points between wide and narrow segments alternately drift downstream, become pinned, and move again. Occasionally, a wide segment will disappear as two necks coalesce. This stick-slip behavior is nonperiodic. The thresholds for time dependence are denoted $Q_t^+$ and $Q_t^-$, depending on whether the flow rate is being increased for decreased.

For a typical angle of 19°, the thresholds are $Q_{CW}=0.05$ $cm^3$ s, $Q_s=0.19$ $cm^3/s$, $Q_t^-=0.39$ $cm^3/s$, and $Q_t^+=0.68$ $cm^3/s$. The variation with angle is weak, and the sensitivity to wetting properties leads to some variation over long periods of time. For this reason, we do not present a parameter space diagram of the various regimes as a function of angle and flow rate; this would convey an impression of greater precision than the observations warrant.

The spatial width modulation is somewhat reminiscent of the initial stages of the capillary instability of a liquid jet,[18] but in our case the driving mechanism is not the surface tension of the air-water interface, but rather the multivalued contact angle at zero velocity. We have checked this hypothesis by repeating the experiment with clean glass plates. In this case, the water jets the plates independent of velocity, and the stream flows without width modulation. Streamline visualization using Kalliroscope particles shows that the flow comes out of the necks into the wide regions as a jet with slow recirculation zones on either side of it. The jet may play a role in the initiation of the contact line motion, but we have not investigated this point. The typical fluid velocity, which is dependent on both flow rate and stream width, is on the order of 20 cm/s in the neck regions and as little as a third that in the wide regions. Using the thickness $b$ of the cell as a typical length scale, and the jet velocity as a velocity scale, the Reynolds number is typically 500–1000, depending on the flow rate.

## IV. COMPLEX SPATIOTEMPORAL REGIME

The complex nature of the time-dependent regime is illustrated in Fig. 6. Here, the stream width [actually $w_0-w(x,t)$, with $w_0$ a constant] is shown as a function of $x$ and $t$. The necks appear as peaks drifting downstream at a characteristic velocity. Some additional features of the long-time behavior in the time-dependent regime may be better appreciated in Figs. 7(a) and 7(b). These are intensity-coded plots of $w(x,t)$ at two different $Q$ values; Fig. 7(a) represents a state of the system very close to $Q_t^+$, while Fig. 7(b) was obtained at higher $Q$. In these figures, the intensity is proportional to $w(x,t)$, so

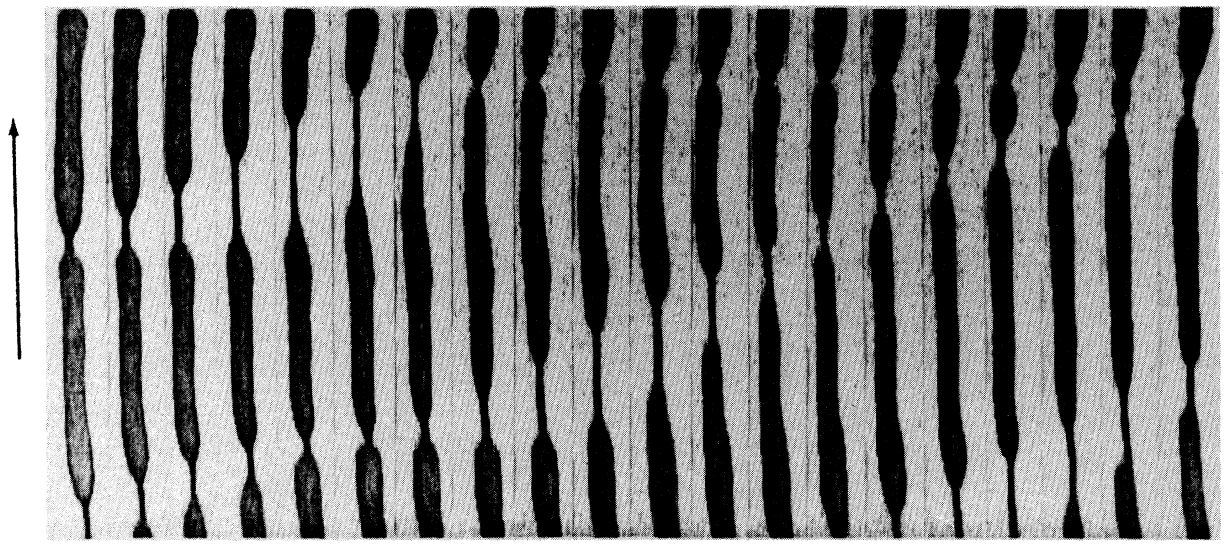

FIG. 5. Consecutive images in the time-dependent regime at $\alpha = 14°$, and $Q = 0.86$ cm$^3$/s. The images are separated by $\frac{1}{6}$ s. The region shown is 13 cm long, and the fluid is flowing from bottom to top, as indicated by the arrow.

dark bands represent necks and bright bands represent wide regions. The necks may be seen to stop and remain at rest for some time (vertical lines), after which they begin to move again. Furthermore, they sometimes stick until other necks arrive, giving rise to coalescence of segments.

Some insight into the statistics of the time-dependent regimes can be gained by observing the local behavior of the width, $w(x_0,t)$. In Fig. 8(a) we show the time evolution of the local stream width just above $Q_t^+$. $W(t)$ oscillates irregularly between two quite-well-defined values that correspond to the width of the wide and narrow regions, respectively. This main oscillation has an average period of about 1.2 s that is related to the length of the segments and the drift velocity of the necks. More time is spent at the larger width, a consequence of the fact that the wide regions are longer than the necks. The nonperiodic nature of the time dependence is clearly seen in the power spectrum [Fig. 8(b)], which is broadband but has a visible hump near 0.8 Hz corresponding to the mean drift rate past the observation point.

Figure 9 shows the same quantities at higher $Q$, far above the transitions. The characteristic frequency is higher (because the fronts move more quickly), and the

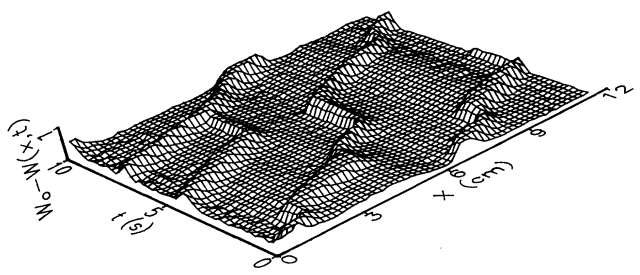


FIG. 6. Three dimensional plot of $w_0$-$w(x,t)$ as a function of position and time at $\alpha = 14°$, and $Q = 0.50$ cm$^3$/s. The necks appear as propagating bumps.

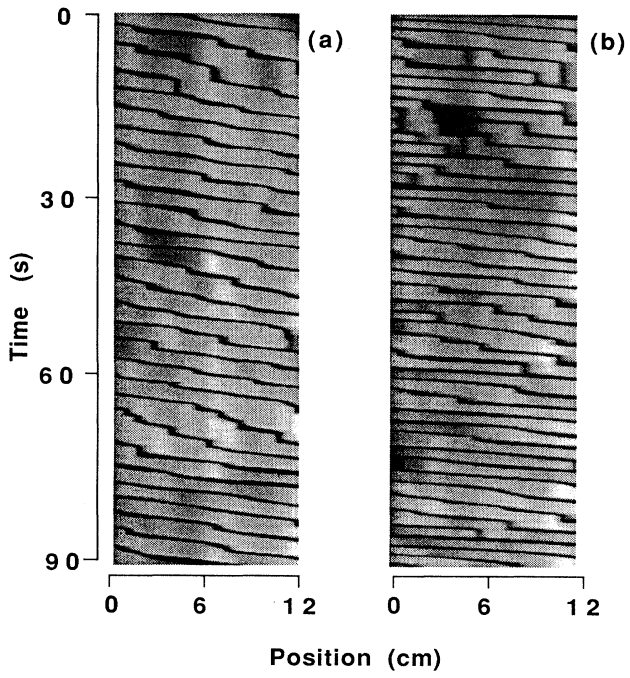


FIG. 7. Intensity-coded plot of $w(x,t)$. (a) Stick-slip regime at $\alpha = 14°$, and $Q = 0.50$ cm$^3$/s; (b) higher flow rate, $Q = 0.80$ cm$^3$/s.

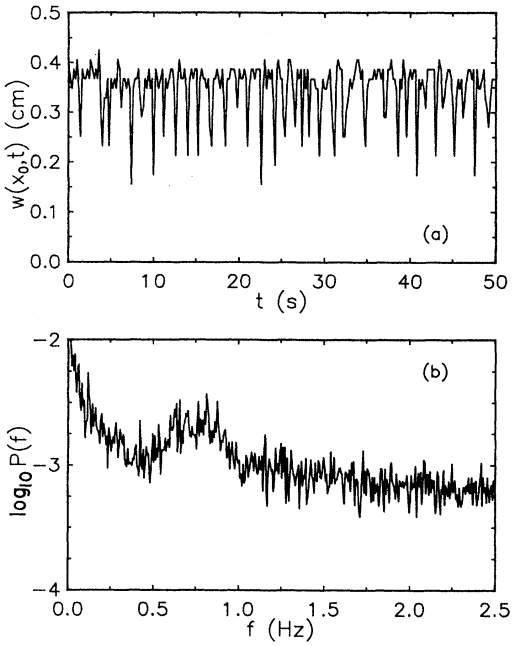


FIG. 8. Local temporal behavior just above the onset of front motion $Q_t^+$ (at 0.62 cm$^3$/s), with the inclination set at $\alpha=19°$. (a) Time series. (b) Power spectrum.

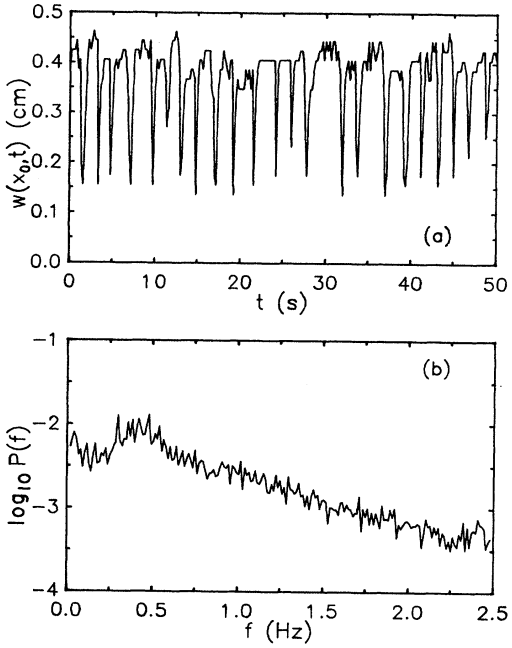


FIG. 10. Local temporal behavior at $Q=0.44$ cm$^3$/s, just above flow rate $Q_t^-$ at which time dependence ceases upon decreasing $Q$. (a) Time series of the local width $w(x_0,t)$. (b) Power spectrum.

motion is somewhat more regular since the pinning is less prominent. Figure 10 pertains to the state reached after *decreasing* $Q$ to a value just above $Q_t^-$. In this region the mean frequency is significantly lower and the peak is broader, as the pinning process occurs much more frequently.

The basic pinning phenomenon can be illustrated by measuring the dependence on $Q$ of the mean interval $\tau$ between passage times of necks past a fixed position $x$. This relationship is shown in Fig. 11. The strong increase in $\tau$ close to $Q_t^-$ is caused by the interfacial pinning. The time interval appears to diverge at the threshold. Through a power-law exponent of approximately $-\frac{1}{3}$ can be computed for the divergence, the exponent is imprecise due to uncertainty in $Q_t^-$.

An alternate method of describing the pinning dynamics is to follow the motion of the leading and trailing

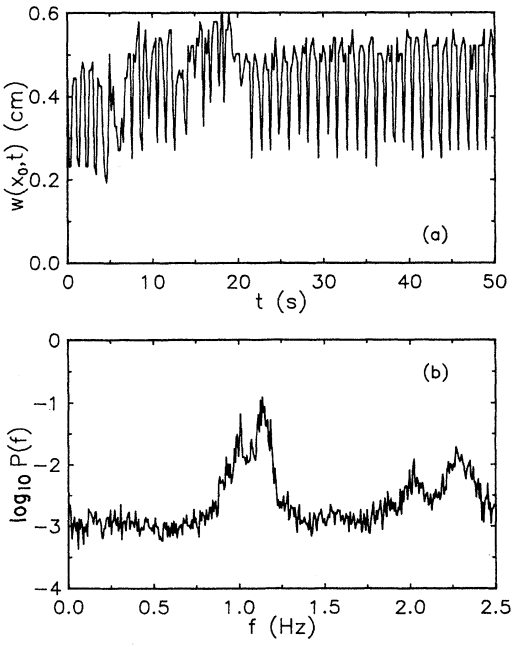


FIG. 9. Local temporal behavior at a higher flow rate ($Q=1.15$ cm$^3$/s). (a) Time series of the local width $w(x_0,t)$. (b) Power spectrum.

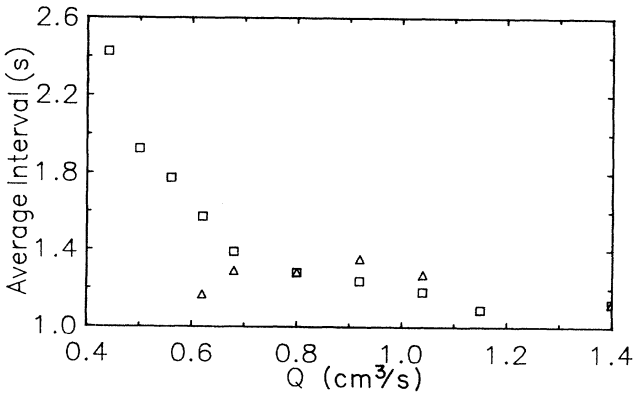


FIG. 11. (a) Average time interval between passage times of successive necks past a fixed point $x$ vs $Q$ at $\alpha=19°$: squares, decreasing $Q$; triangles, increasing $Q$.

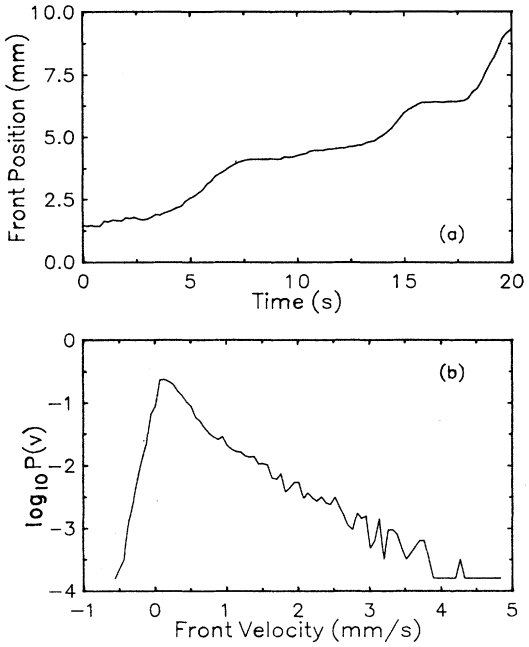


FIG. 12. (a) Front position as a function of time. $\alpha = 14°$; $Q = 0.39$ cm$^3$/s. (b) Probability distribution of front velocities.

fronts separating a wide segment from the adjacent necks. An example of the trajectory of a front in the region just above $Q_t^-$ is shown in Fig. 12(a). The pinning process is quite evident. The probability distribution of front velocities is shown in Fig. 12(b). It shows a peak near $v = 0$ (corresponding to the pinning), and a broad distribution above that. This behavior implies that the front motion does not occur at a single predominant velocity, but instead varies with time.

## V. DISCUSSION AND CONCLUSION

### A. Width modulations

We find that uniform streams confined between two parallel plates are unstable above a certain flow rate $Q_s$, and have presented evidence that this behavior occurs when the contact angle is multivalued at zero velocity. A width-modulated stationary state arises above the instability threshold, with an average wavelength that decreases as the inclination $\alpha$ of the plates increases.

The existence of the width-modulation instability may possibly be understood by considering the fact that the local contact angle is dependent on the local pressure drop $\Delta p$ across the interface according to the relationship

$$\theta = \cos^{-1}\left[\frac{b\Delta p}{2\gamma}\right].$$

The local pressure in turn is affected by the gravitational, viscous, and dynamic pressure drops within the stream. If these become sufficiently large, the critical angle $\theta_c$ for motion of the contact line may be exceeded, causing the interface to translate in a direction transverse to the stream, and thereby changing the local interfacial width.

However, a stability analysis is required to actually determine the threshold and most unstable wavelength $\lambda_c$. We attempted to measure $\lambda_c$ as a function of the mean stream width, but the scatter was too large to reveal a meaningful relationship. Some preliminary efforts at a stability analysis of this phenomenon have been made.[19]

### B. Spatiotemporal dynamics

Above a higher (and hysteretic) transition, a complex spatiotemporal regime appears in which the water-air-solid contact line becomes time dependent. We characterized the spatiotemporal dynamics above this transition in several different ways. The most striking observation is the repetitive but nonperiodic pinning of the fronts for times that appear to diverge near the lower threshold $Q_t^-$. The stick-slip dynamics of the front motion, once the fronts have formed, may possibly be understood approximately by a simple model in which the pressure at each front is described by the sum of the gravitational and viscous pressure drops in the various segments. As the stream is traversed in the downstream direction, the pressure increases in the wide segments due to gravity, but drops in the necks due to the dominance of viscosity in those regions. As a result, the local pressure varies, and exceeds the threshold pressure required for contact line motion only in certain locations. The various fronts interact, because their locations determine the lengths of the narrow segments, which affects the viscous pressure drops. One unrealistic feature of such a model is that it ignores any possible connection between the process that creates the fronts in the first place and the dynamics of their motion.

It may be interesting to compare the statistical behavior of this system with that of the other systems mentioned in Sec. I. Is the dynamical behavior of the fronts analogous to the stick-slip dynamics of the blocks in the simplified earthquark models of Ref. 9? In both cases, there is a threshold condition for forward motion in a chain of objects that interact with each other. Both systems show broadband temporal dynamics. There are also differences; the blocks in the earthquake models are conserved, whereas the fronts are not. The statistical quantities studied in the two cases are also somewhat different. Carlson and Langer focus on the distribution of magnitudes of events, as defined by the number of blocks that move. In the stream experiments, this quantity would be hard to define, since the size of the system is sufficient to include only a small number of fronts, and the present experiments have not been done close enough to $Q_t^-$ to produce clearly isolated localized events. It would be worthwhile in future experiments to work very close to $Q_t^-$. In addition, if the two systems are similar, we would expect the slipping events in the earthquake model to become more nearly periodic as the pulling rate is increased. It would be interesting to know whether this is the case.

## ACKNOWLEDGMENTS

This research was supported by the National Science Foundation (Low-Temperature Physics Program) Grant No. DMR-89-01869. S. Kane provided important experimental assistance. We thank D. A. Kessler and H. Levine, and E. B. Dussan V for helpful discussions. We also appreciate equipment provided by the U.S. Department of Defense University Research Initiative Program under Contract No. DARPA/ONR-N00014-85-K-0759 to Princeton University.

[1]Y. Chaté and P. Manneville, Phys. Rev. Lett. **58**, 112 (1987).
[2]S. Ciliberto and P. Bigazzi, Phys. Rev. Lett. **60**, 286 (1988).
[3]F. Daviaud, P. Bergé, and M. Dubois, Europhys. Lett. **9**, 441 (1989).
[4]For a review of recent experiments and models, see J. P. Gollub and R. Ramshankar, in *New Perspectives in Turbulence,* edited by S. Orszag and L. Sirovich (Springer-Verlag, Berlin, 1991).
[5]P. Bak, C. Tang, and K. Wiesenfeld, Phys. Rev. A **38**, 364 (1988).
[6]H. M. Jaeger, C. Liu, and S. R. Nagel, Phys. Rev. Lett. **62**, 40 (1989).
[7]P. Evesque and J. Rajchenbach, Phys. Rev. Lett. **62**, 44 (1989).
[8]G. William Baxter, R. P. Behringer, Timothy Fagert, and G. Allan Johnson, Phys. Rev. Lett. **62**, 2825 (1989).
[9]J. M. Carlson and J. S. Langer, Phys. Rev. Lett. **62**, 2632 (1989); Phys. Rev. A **40**, 6470 (1989).
[10]Z. Cheng, S. Redner, P. Meakin, and F. Family, Phys. Rev. A **40**, 5922 (1989).
[11]G. Grüner and A. Zettl, Phys. Rep. **119**, 117 (1985).
[12]D. S. Fisher, Phys. Rev. A **31**, 1396 (1985).
[13]S. H. Strogatz, C. M. Marcus, R. M. Westervelt, and R. E. Mirollo, Phys. Rev. Lett. **61**, 2380 (1988); Physica **36D**, 23 (1989).
[14]E. B. Dussan V, J. Fluid Mech. **77**, 665 (1976).
[15]K. M. Jansons, J. Fluid Mech. **154**, 1 (1985); **167**, 393 (1986).
[16]T. Nakagawa and J. C. Scott, J. Fluid Mech. **149**, 89 (1984); R. Bruinsma (private communication); T. Maxworthy, Bull. Am. Phys. Soc. **34**, 2265 (1989).
[17]C. G. Ngan and E. B. Dussan, J. Fluid Mech. **118**, 27 (1982).
[18]See, for instance, S. Chandrasekhar, *Hydrodynamic and Hydromagnetic Stability* (Dover, New York, 1961); or P. G. Drazin and W. H. Reid, *Hydrodynamic Stability* (Cambridge University, Cambridge, England, 1981).
[19]D. A. Kessler and H. Levine (private communication).

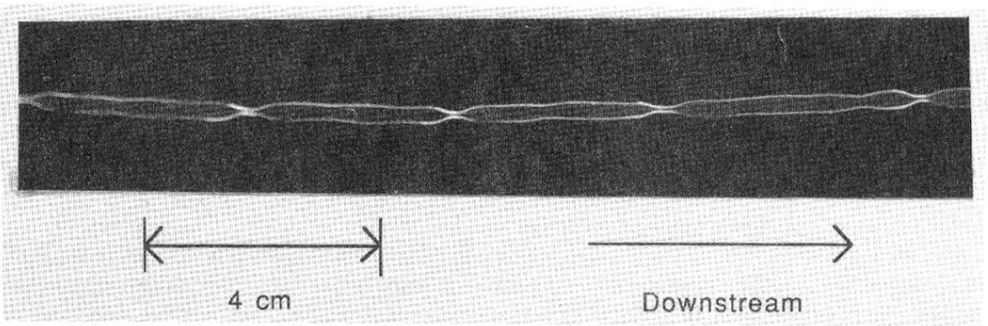


FIG. 1. Photograph of the stream in the stationary modulated regime. The angle of inclination is $\alpha = 19°$, and the flow rate is $Q = 0.28\ \text{cm}^3/\text{s}$.

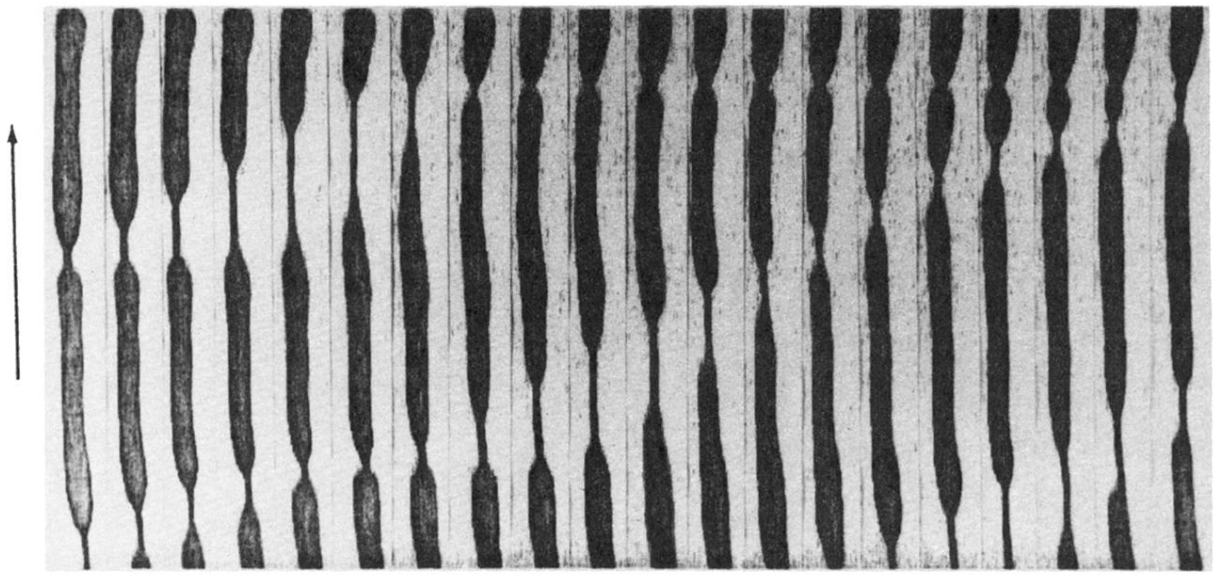

FIG. 5. Consecutive images in the time-dependent regime at $\alpha = 14°$, and $Q = 0.86$ cm$^3$/s. The images are separated by $\frac{1}{6}$ s. The region shown is 13 cm long, and the fluid is flowing from bottom to top, as indicated by the arrow.

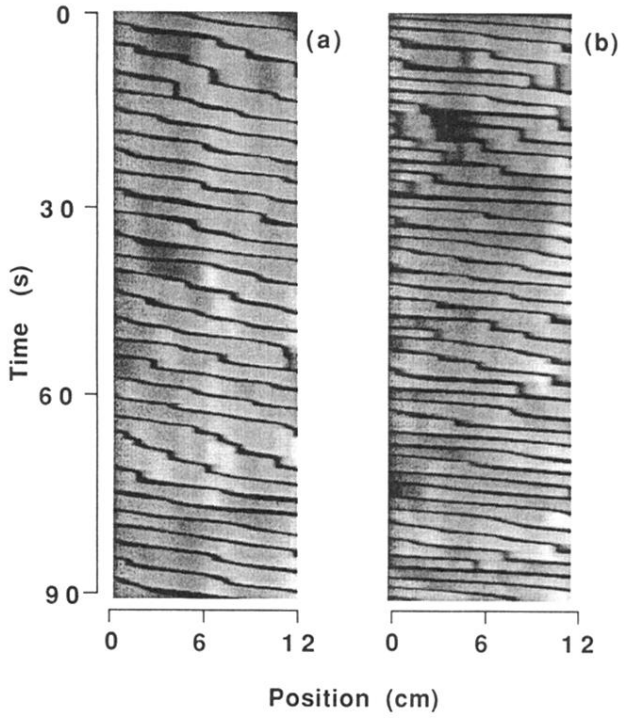


FIG. 7. Intensity-coded plot of $w(x,t)$. (a) Stick-slip regime at $\alpha=14°$, and $Q=0.50$ cm$^3$/s; (b) higher flow rate, $Q=0.80$ cm$^3$/s.